The fluid dynamics of flight control by kinematic phase lag variation between two robotic insect wings

Will J. Maybury and Fritz-Olaf Lehmann*

Department of Neurobiology, University of Ulm, Albert-Einstein-Allee 11, 89081 Ulm, Germany

*Address for correspondence (e-mail: fritz.lehmann@biologie.uni-ulm.de)

Summary

Insects flying with two pairs of wings must contend with the forewing wake passing over the beating hindwing. Some four-winged insects, such as dragonflies, move each wing independently and therefore may alter the relative timing between the fore- and hindwing stroke cycles. The significance of modifying the phase relationship between fore- and hindwing stroke kinematics on total lift production is difficult to assess in the flying animal because the effect of wing–wake interference critically depends on the complex wake pattern produced by the two beating wings. Here we investigate the effect of changing the fore- and hindwing stroke-phase relationship during hovering flight conditions on the aerodynamic performance of each flapping wing by using a dynamically scaled electromechanical insect model. By varying the relative phase difference between fore- and hindwing stroke cycles we found that the performance of the forewing remains approximately constant, while hindwing lift production may vary by a factor of two. Hindwing lift modulation appears to be due to two different fluid dynamic phenomenons: leading edge vortex destruction and changes in strength and orientation of the local flow vector. Unexpectedly, the hindwing regains aerodynamic performance near to that of the wing free from forewing wake interference, when the motion of the hindwing leads the forewing by around a quarter of the stroke cycle. This kinematic relationship between hind- and forewing closely matches the phase-shift commonly used by locusts and some dragonflies in climbing and forward flight. The experiments support previous assumptions that active neuromuscular control of fore- and hindwing stroke phase might enable dragonflies and other functionally four-winged insects to manipulate ipsilateral flight force production without further changes in wing beat kinematics.

Key words: insect flight, aerodynamics, DPIV, leading edge vortex, wake, dragonfly.

Introduction

Functionally four-winged insects such as dragon- and damselflies use a large variety of wingbeat kinematics to produce and control aerodynamic forces for flight (Alexander, 1984; Azuma et al., 1985; Azuma and Watanabe, 1988; Chadwick, 1940; Grodnitsky and Morozov, 1992; Reavis and Luttges, 1988; Rüppell, 1989; Rüppell and Hilfert, 1993; Sato and Azuma, 1997; Somps and Luttges, 1985; Wakeling, 1993; Wakeling and Ellington, 1997; Wang et al., 2003; Weis-Fogh, 1967). The neuromuscular system allows these animals to actively manipulate many aspects of wing motion such as stroke amplitude, stroke frequency, the angle of attack and stroke plane (Norberg, 1975; Rüppell, 1989), but also to actively control the timing between the fore- and hindwing stroke cycles (kinematic phase relationship, Alexander, 1984; Azuma and Watanabe, 1988; Clark, 1940; Grodnitsky and Morozov, 1992; May, 1995; Sato and Azuma, 1997; Simmons, 1977a,b; Wakeling and Ellington, 1997; Wang et al., 2003). Thus dragonflies and damselflies differ significantly from other four-winged insect species such as butterflies, bees, wasps and

ants, whose fore- and hindwings always beat in phase, due to a sophisticated joint that mechanically couples the motion of both wings throughout the entire stroke cycle (Gorb, 2001). Other insects of more primitive orders, such as locusts, lie somewhere between both extremes; in locust, the stroke-phase relationship seems to be highly consistent, with little variation during flight control (Chadwick, 1953; Weis-Fogh, 1956; Wilson, 1968; Wortmann and Zarnack, 1993). Cooter and Baker (1977) reconstructed wing motion of freely flying locust *Locusta migratoria* and found a fixed phase relationship between their fore- and hindwings in which the forewing slightly leads by approximately 61°.

In contrast, dragonflies vary the phase relationship between ipsilateral fore- and hindwings with different behaviors (Norberg, 1975; Reavis and Luttges, 1988; Wakeling and Ellington, 1997; Wang et al., 2003). Three categories of phase relationship between fore- and hindwing have been established: phase-shifted stroking, counterstroking and parallel stroking. A highly consistent characteristic for the

conventional flight modes is a 54–100° phase shift (the hindwing leads forewing motion) common for dragonflies during (i) straight forward and upward flight, (ii) the escape mode, in which a tethered animal produces peak lift in each stroke cycle of up to approximately 20 times their body weight, and (iii) during maneuvering flight (Somps and Luttges, 1985; Wakeling and Ellington, 1997; Wang et al., 2003). The kinematic phase shift persists even when the animals are changing forward flight speed (Wakeling and Ellington, 1997). In contrast, hovering flight seems to be supported by larger phase differences of up to 180°, in which the wings beat out of phase (counterstroking; Alexander, 1986; Norberg, 1975; Wakeling and Ellington, 1997). Counterstroking was also found in a study on maneuvering flight in dragonflies flying freely in a wind tunnel (Alexander, 1986). Detailed analysis of wing kinematics during various flight behaviours suggests that in-phase, or parallel stroking, might produce higher aerodynamic forces and should be favored during the energetically most demanding flight such as hovering, take-off or load-lifting flight (Alexander, 1984, 1986; Rüppell, 1989).

Direct force measurements on tethered dragonflies flying in a wind tunnel show that peak lift increases from approximately 2.3 to 6.3 times body weight when the animal decreases the phase angle between both flapping wings (Reavis and Luttges, 1988). Although this finding supports the assumption that parallel stroking might maximize lift production, it has been questioned by analytical modeling in which flight efficiency and mean thrust coefficient was estimated as a function of kinematic phase relationship (Lan, 1979). This study predicts that the hindwing extracts maximum energy from the forewing downwash when the hindwing leads by a quarter stroke cyle (90°), while the thrust coefficient is largest when the phase relationship is 45°. As a consequence, dragonflies exhibiting parallel stroking will increase thrust, but at the expense of a relative increase in energetic costs.

According to biplane theory, total lift production in tandem wings depends on the proximity and the strength of forewing downwash that interferes with the hindwing (Milne-Thomson, 1966). In dragonflies, the hindwing flaps in close proximity to the forewing and thus must cope with a potential reduction in the effective angle of attack (the angle between the wing chord line and the oncoming fluid) due to forewing downwash. The attenuation in aerodynamic performance of the hindwing in turn critically depends on forewing wake structure and the timing with which the hindwing interacts with the forewing downwash (Azuma et al., 1985). Assuming two-dimensional (2D) flapping conditions, two long and narrow wings working independently should have higher lift-to-drag ratios than a combined wing with the same wing area, due to the differences in aspect ratio (Bertin and Smith, 1979; Mises, 1959). Thus tandem wings flapping in phase should produce less total lift because the two wings are always closer throughout the entire stroke cycle than wings flapping out of phase (Alexander, 1984).

It is difficult to assess the significance of phase relationship to modulate lift production in a flying insect because kinematic phase shifts are mostly accompanied by other changes in wing kinematics, such as stroke amplitude or angle of attack (Reavis and Luttges, 1988; Wakeling and Ellington, 1997). For this reason various investigations on the aerodynamics of static and flapping dragonfly and damselfly wings have been conducted under various conditions, either experimentally (Kesel, 2000; Kliss et al., 1989; Newman et al., 1977; Okamoto et al., 1996; Saharon and Luttges, 1987; Somps and Luttges, 1985) or analytically (e.g. Azuma et al., 1985; Wang et al., 2003). Savage et al. (1979) modeled dragonfly aerodynamics experimentally under 2D conditions by pulling a single model wing on a carriage through the air, and derived forces from the resulting wake using inviscid flow theory. Kliss et al. (1989) used an oscillating flat plate with 90° angle of attack to study vortex shedding, and found that stroke length is critical to minimize complete flow separation during wing translation. In several elaborate studies, Saharon and Luttges (1987, 1988, 1989) demonstrated vortex generation in a mechanical-driven dragonfly under three-dimensional (3D) flapping conditions and described eight major vortices that are generated throughout each wing beat cycle. They found that in most of the tested cases, much of the interference between hindwing and forewing wake was detrimental to maximized wing–wake interaction. Different stroke-phase relationships (90, 180 and 270°) produced different flow wing–wake patterns, and vortices appeared to fuse under certain flapping conditions. A quantitative analysis of vortex displacement in the wake revealed that the travelling velocity of some vortices shed in the wake varied when phase relationship was altered (Saharon and Luttges, 1989). However, none of the studies mentioned above have directly measured aerodynamic forces produced by the flapping fore- and hindwing, nor quantified alterations in leading edge vorticity and local flow conditions in response to changing kinematic phase angles.

To investigate experimentally the complex wing–wake interaction in four-winged insects and to evaluate in more detail the functional significance of stroke-phase modulation on wake structure, aerodynamic force production and lift-to-drag ratio, we employed a 3D robotic dragonfly model mimicking hovering conditions at intermediate Reynolds number, in which stroke-phase relationships between fore- and hindwing could be altered systematically. While varying kinematic phase shift we measured aerodynamic forces using a miniaturized force transducer, and mapped the velocity field around the flapping wings using Digital Particle Imaging Velocimetry (DPIV) in order to quantify vorticity and vortical flow structures at the wings, including the structures shed into the wake.

Materials and methods

To experimentally assess the gross effects on wing lift force due to modulation of fore- and hindwing stroke phase in four-winged flight, we modeled the wing–wake interaction during hovering flight of a dragonfly using a dynamically scaled electromechanical model of the right side of a four-winged

insect and employing a generic kinematic pattern described below (Fig. 1B,D). The model wings were each equipped with a 6-DoF force transducer to measure instantaneous aerodynamic force production, while we systematically varied the kinematic phase relationship between the wings in steps of 2.5% of the stroke cycle. In addition to the force measurements we quantified the flow characteristics around the hindwing using 2D-DPIV for the two kinematics phase shifts that produce the maximum and minimum modulation in hindwing lift at two key times within the stroke cycle.

Development of a generic kinematics and wing control

Owing to the range of stroke patterns used by dragonflies to balance their weight and allow maneuvering, it appears to be difficult to describe a typical dragonfly kinematics (Norberg, 1975; Rüppell, 1989). Kinematic studies on different species of dragonfly demonstrate that during forward and climbing flight some animals beat their wings with a near horizontal stroke plane (Wakeling and Ellington, 1997; Fig. 1A) and others with highly inclined stroke planes (Azuma and Watanabe, 1988; Wang et al., 2003). Moreover, dragonflies produce flight forces using various combinations of stroke amplitude and stroke frequency that range from 50 to 150° and from 27 to 73 Hz, respectively (Azuma and Watanabe, 1988; Rüppell, 1989).

Due to this diversity of dragonfly kinematics, various authors have modeled physically and analytically different types of dragonfly kinematics. In the oscillating flat plate case (Kliss et al., 1989), the authors varied stroke amplitude, frequency and aspect ratio, but did not model other characteristic features of dragonfly wing motion, including wing–wake interaction. The study, moreover, compared aerodynamic flow patterns produced over a vast range of Reynolds numbers (*Re*) ranging from 10 to 4300. Savage's physical model (Savage et al., 1979) of a hovering dragonfly used Norberg's kinematic data of freely flying dragonfly *Aeschna* (Norberg, 1975). This model wing did not flap its wing around a root, however, but rather translated during up- and downstroke. The more elaborate 'pitching–plunging' dragonfly model employed by Saharon and Luttges (1988, 1989) flapped two ipsilateral wings in a tilted stroke plane and at 90° stroke amplitude. In this model the authors varied reduced frequency, which was accompanied by changes in *Re*, and three distinct phase angles between fore- and hindwing, but no other kinematic parameters (Saharon and Luttges, 1989). Aerodynamic characteristics of static dragonfly wings and body were conducted under 2D conditions in a wind tunnel (Kesel, 2000; Okamoto et al., 1996). In the latter study the authors mounted wings of a dragonfly and flat plates on a glider and evaluated the effect of angle of attack (dragonfly wing), camber, thickness sharpness of the leading wing edge and surface roughness (model wing) on force production at *Re*=1000–10 000.

To avoid too many kinematic parameters confounding the results in the present study, we developed a generic kinematic pattern that allowed us to model kinematic phase shifts similar to those reported for dragonflies (Fig. 1B). The horizontal wing

trajectories were derived from a simple sinusoidal function, which was chosen because of a finding in previous studies that the first harmonic of a Fourier series gives a good representation of the stroke cycle of freely flying dragonflies (Azuma and Watanabe, 1988; Wakeling and Ellington, 1997; Wang et al., 2003). We used a constant angle of attack during wing translation with a feathering angle of 45° at mid stroke, which is similar to values reported previously (Azuma and Watanabe, 1988; Fig. 2B). This angle is the optimum lift angle of a translating wing free from wake interference and is within the range of data published for dragonflies (Dickinson et al., 1993; Rüppell, 1989). The stroke amplitude of 100° that we used is near the average measured for both the fore- and hindwing motion in dragonflies flying at various flight speeds (Wakeling and Ellington, 1997). The flapping frequency of the robotic wings was 533 mHz.

We chose to stack the wings vertically, which seems to be sufficiently close to the orientation of wing hinges presented by a freely flying dragonfly with a near vertical mean thrust vector (Fig. 1A,B). In this respect our tandem model with vertical aligned wings differs from other dragonfly models in which the wing hinges are aligned horizontally, yielding a 'front' and a 'rear' wing rather than an 'upper' and a 'lower' wing (Saharon and Luttges, 1987, 1988). For this reason, our model only covers a limited aspect of four-winged insect flight. It is not intended to explain *per se* the various types of wing–wake interaction assumed during the various forward and hovering flight conditions found in freely flying dragonflies. If not stated otherwise, fore- and hindwing hinges in our robotic model were separated vertically by 1.3 mean forewing chord lengths, i.e. the closest distance between the wings at which the wings did not touch physically during flapping at the various kinematic phase relationships (Fig. 1C).

In accordance with the stroke kinematics used for an analytical dragonfly model, we chose a symmetrical wing rotation during the ventral and dorsal stroke reversal, in which the midpoint of rotational duration occurs when the wing reverses its translational direction (Wang, 2000a). A wing rotating symmetrically starts rotating before and finishes after it has reversed its flapping direction, which may minimize rotational lift because at that time translational wing velocity is smallest. To minimize inertial load produced by rotational moments in our generic kinematic pattern, wing rotation followed a sinusoidal velocity profile. The onset of wing rotation relative to stroke reversal, expressed as a fraction of the total wing cycle time, τ_0, was –0.1, indicating that wing rotation begins 10% of the stroke period prior a stroke reversal. Flip duration, $\Delta\tau$, was 0.2, indicating that wing rotation ends 10% after the stroke reversal (for nomenclature, see Sane and Dickinson, 2001a). The kinematic pattern we used in this study produces lift due to wing rotation equivalent to 3.2% of total lift production by the hindwing free from forewing wake interference. We estimated rotational lift contribution from total lift by subtracting the 'quasi-steady' lift estimate during wing translation that was calculated using a conventional 'quasi-steady' analytical model, as suggested by Dickinson et

al. (1999). In sum, considering the small amount of rotational lift, it seems unlikely that the pronounced modulation in measured hindwing lift production as shown in the present study results from alterations in rotational circulation during the stroke reversals, but rather reflects aerodynamic mechanisms during wing translation.

The motion of the two model wings was driven by six servo motors that are controlled by self-written software developed under Visual C++.NET (Microsoft) for a conventional computer. To record force data and to control wing motion simultaneously, the computer was equipped with a 16-channel analog-to-digital data acquisition board (6036E, National Instruments, Austin, TX, USA) and a 24-bit digital interface card (6503, National Instruments) for controlling the motion of the servo motors *via* a micro-controller (Fig. 1C). We updated the angular position of the entire motor assembly with a maximum rate of 67 Hz (0.015 ms period), whereas the force sampling frequency was approximately 12-times higher, yielding 800 Hz. A potential problem during wing motion of robotic wings is that the actual wing kinematics may differ from the programmed kinematic pattern, whenever the actual power requirements for wing motion exceed the power supplied by the driving motors. This happens especially when the wings accelerate from rest under high inertial load. To avoid a confounding effect on our force measurements due to power constraints of the motor assembly, we modified the servo motors in order to monitor electrically their internal angular position, which is mechanically determined by the angle of the motor main shaft driving the wing. In a control procedure preceding each experimental series, we compared the actual angular position of each servo motor with the programmed wing angles and adjusted either the motor's power supply or the wing's flapping frequency until actual and programmed kinematics were indistinguishable. Besides other constraints, the high power requirement for wing flapping was a major factor that limited maximum flapping speed, and thus *Re*, of our model wings.

In addition to kinematic modifications of wing motion due to power constraints, wing kinematics may also change due to wing flexing and bending. Moreover, wing flexing can potentially produce inertial peaks that might complicate the measured force traces. Although inertial forces produced during the acceleration and deceleration periods of the wing are relatively small (see below and Fig. 2A), strong flexing of the wing might add brief periods of acceleration/deceleration components to the overall wing acceleration/deceleration profile that is produced by the translational and rotational wing motion. Fig. 2B shows that the hindwing flapping free of the forewing downwash experiences a maximum combined aerodynamic and inertial load between 0.4 and 0.6 N for each mid-halfstroke. To derive a rough estimate of the magnitude of wing flexing during the various times of the stroke cycle, we statically loaded the wing in air with small weights that we placed either at a distance of two-thirds wing length on the upper wing surface or at the wing tip, and measured the deflection of the wing at both locations (Fig. 1D). Loading the

wing at the wing tip is thought to produce a rather conservative estimate because the main force vector during wing translation is thought to act close to the two-thirds wing position. The results show that with an average load of 0.3 N, which is equal to the average force measured throughout the entire stroke cycle, fore- and hindwing solely flex approximately 1.0 mm at two-thirds distance from the wing holder, and up to 1.7 mm under the maximum load of 0.5 N that occurs approximately at mid-halfstroke. Due to the sinusoidal velocity profile during wing translation, however, we assume that the wing builds up and releases its deflection more gradually at the beginning and the end of each halfstroke, respectively, which should in turn minimize sudden accelerations and thus high inertial peaks. In sum, we feel rather confident that the measured alteration in force development due to the various kinematic phase shifts between fore- and hindwing are not primarily caused by extensive wing flexion but are likely to represent aerodynamic alterations due to wing–wake interaction.

Force measurements

Fore- and hindwing planforms were based on the wings of the dragonfly *Polycanthagyna melanictera* Selys and were made from 2 mm Plexiglas. Since wing velocity of each wing blade element depends on its distance to the rotational axis of the robotic hinge, we calculated total wing length as the distance between the vertical rotational axis of the gear box and wing tip. Thus total forewing length was 190 mm with an aspect ratio of 6.8, and total hindwing length was 185 mm with an aspect ratio of 7.4, assuming that gear box, force sensor and wing holder add to wing length but not to wing area (Fig. 1C). However, the length of the wings *sensu strictu* (without wing holder, force sensor and gear box) was only 135 mm for the upper forewing (aspect ratio=3.6) and 140 mm for the lower hindwing (aspect ratio=4.2; Fig. 1C). Each wing was mounted on a robotic hinge with three-degrees of freedom, with all axes crossing a single origin.

In this study we modeled hovering flight conditions of a four-winged insect, which are thought to differ from flow conditions produced during steady forward flight. Advanced ratio as well as reduced frequency are ratios of the 'steady motion' caused by the body of an insect flying through the air at constant speed, whereas 'unsteady motion' is due to motion of a wing oscillating back and forth about its root. Advanced ratio and reduced frequency are thus measures that indicate which velocity component (free stream due to body motion or wing flapping) dominates the incident flow on the wing. Both quantities are important for 'quasi-steady' analytical modeling and the development of dynamically scaled robotic hinges. Since we modeled hovering flight conditions, however, all flow components acting on the two wings are generated by the wing's own motion and thus advance ratio is zero and reduced frequency is infinity.

The two scaled wings were immersed in a 0.6 m×0.6 m×1.2 m glass tank filled with pharmaceutical white oil (density, $0.88×10^3$ kg m^{-3}; kinematic viscosity, 120 cSt). The size of the tank was chosen to minimize wall and

ground effects that were calculated based on a set of equations derived from a robotic wing flapping in oil at similar speed (Dickinson et al., 1999). A modified force/torque sensor (Nano17, ATI, Apex, NC, USA) was alternately attached to the base of each wing, and the experiments were repeated to obtain measurement on both wings. The sensor recorded shear forces and moments along and around all three wing axes. We converted forces measured normal and parallel to the wing surface into lift and drag using commercial Active-X controls (ATI) and software written in Visual C++.NET. We typically recorded six successive stroke cycles. It has been shown that the first stroke cycle produces slightly higher forces because the downwash velocity is minimal under these conditions (Birch and Dickinson, 2001). For further data analysis we thus averaged only four stroke cycles (cycles 2–5) in order to avoid confounding effects from the initial downwash acceleration or any transient forces when the wing was started or halted at the end of the experiment. Mean total force, lift and drag were averaged subsequently throughout the entire stroke cycle. The force traces showing the maximum modulation in lift performance were filtered using a 5 Hz FFT smoothing filter in Origin 7.0 (Microcal, Northampton, MA, USA).

To derive mean lift coefficient $\overline{C}_L$, for wing motion from mean lift and drag averaged throughout the entire stroke cycle, we used the equation:

$$\overline{C}_L = \frac{8\overline{L}}{\rho\Phi^2 n^2 R^2 S (\overline{\mathrm{d}\hat{\phi}/\mathrm{d}\hat{t}})^2 \hat{r}_2^2(S)} , \tag{1}$$

which is a modified expression of equation 12 in Ellington (1984c) developed for hovering flying insects exhibiting a horizontal stroke plane (Lehmann and Dickinson, 1998). In this equation $\overline{L}$ is lift of single wing averaged throughout the stroke cycle, ρ is the density of the mineral oil, Φ is stroke amplitude, defined as the angle that the wings cover during wing translation, n is stroke frequency, R is wing length, S is total wing area, $(\overline{\mathrm{d}\hat{\phi}/\mathrm{d}\hat{t}})$ mean square of dimensionless wing velocity and $\hat{r}_2^2$ is the non-dimensional radius of the second moment of wing area that characterizes wing shape (for nomenclature, see Ellington, 1984d). For a sinusoidal velocity pattern for wing translation, mean square of dimensionless wing velocity is 19.7 (Lehmann and Dickinson, 1998) and the non-dimensional radius of the second moment of wing area is 0.36 for the forewing and 0.38 for the hindwing in our dragonfly model. The force coefficients represent means in which all circulatory mechanisms such as Kutta-lift, leading edge vorticity and rotational circulation, including a possible wake–capture momentum transfer, are lumped into a single coefficient (Dickinson et al., 1999).

Wing inertia and added mass effects

In real and model wings the forces at the wing base consist of at least three different components: (i) aerodynamic forces due to both the pressure distribution around the wing and viscous forces in the fluid, (ii) inertial forces due to wing and added mass acceleration, and (iii) gravitational forces. The gravitational component on the force sensor is due to the mass of the wing and was subtracted from the measured forces by

recording the lift component acting on the resting wing at each point of the stroke cycle. We estimated the contribution of inertial forces due to wing mass analytically, assuming that all mass of the wing, m_w, including the mass of the wing holder, is concentrated in the center of wing mass. The center of wing mass we have indicated by a red dot for each wing shown in Fig. 1C. Although the mass of the wing holder is in close distance to the mounting surface of the force sensor, to which all forces and moments refer, its total mass of approximately 7.0 g is about 54% of the mass of the larger forewing and 62% of the smaller hindwing, and should thus be considered for inertial effects. According to Ellington (1984a), inertial forces during flapping flight in the horizontal plane are proportional to the first moment of wing mass m_1 that is equal to:

$$m_1 = m_w R \int_0^1 \hat{m}' \hat{r} \mathrm{d}\hat{r} . \tag{2}$$

In this equation $\hat{m}'$ is normalized wing mass per unit wing length and $\hat{r}$ is the normalized radial position along the wing. Since the wing holder is a complex 3D piece that was difficult to model analytically, we derived the first moment of total wing mass experimentally by balancing the model wing, including the wing holder, on a small pin with an approximately 1 mm^2 support area. The results of these measurements show that the moment arm, l_x, between the force sensor and the wing's center of mass is 48.3 mm for the forewing and 50.8 mm for the hindwing (Fig. 1C). Inertial forces F_h^* associated to accelerations in the horizontal stroke plane are then:

$$F_h^*(t) = m_w l_x \ddot{\phi} , \tag{3}$$

in which ϕ is the angular position of the wing during the stroke and t is time. However, during wing acceleration the force sensor does not solely experience inertial forces produced by the acceleration in angular wing position but also inertial forces due to changes in the angle of attack, because the center of wing mass is not located exactly on the wing's rotational axis. Thus when the wing starts to rotate, the center of wing mass may experience additional accelerations in the horizontal and vertical direction. We experimentally determined the length of the moment arm normal to the wing's rotational axis, l_y, to be 8.6 mm for the forewing and 3.8 mm of the hindwing (Fig. 1C). The horizontal inertial component modifies drag whereas as the vertical acceleration produces inertial forces acting on the lift vector. The relative contributions of rotational acceleration during stroke reversals to horizontal and vertical inertial forces thereby depend on the angle of attack. A wing that starts rotating at a low angle of attack produces more vertical than horizontal inertial force compared to a wing starting at angles near 90°. Rotational inertia adds positive lift when the wing increases angle of attack and adds negative lift when the angle of attack is decreasing. We approximated instantaneous vertical inertial force F_v similar to Equation 3, but also took into consideration the wing's angle of attack α, which yields:

$$F_v(t) = m_w l_y \ddot{\alpha} \cos\alpha . \tag{4}$$

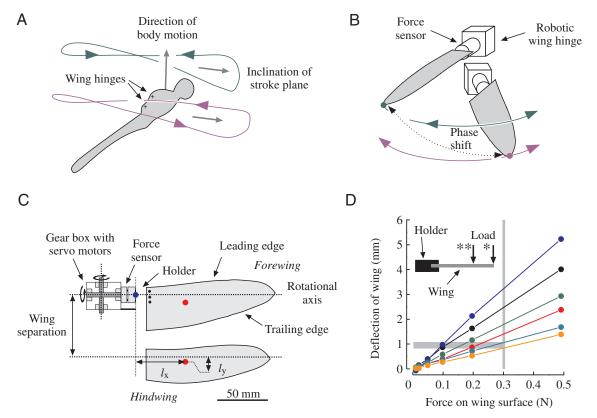Changes in wing acceleration in the horizontal due to changes

Fig. 1. Wing beat kinematics of a dragonfly, set-up of the robotic wing hinge, and mechanical properties of the model wings as used in this study. (A) Diagram showing wing tip path of fore- (green) and hindwing (purple) and orientation of a freely flying dragonfly with near vertical thrust vector. Body orientation, location of the wing hinges and wing tip path were plotted after data published by Wakeling and Ellington (1997). In this kinematic study advance ratio, defined as the ratio between forward and wing flapping speed, was 0.44. Due to the steep body angle with respect to the horizontal, the wing hinges are aligned almost vertically and thus similar to the alignment of the robotic wing hinges shown in (B). (B) Schematic diagram of the robotic dragonfly setup, modeling aerodynamic characteristics on one side of the functionally four-winged insect with the forewing and hindwing wingtip trajectories of our generic dragonfly kinematics superimposed (see Materials and methods for details). The kinematics used during fore- and hindwing motion is identical in all experiments, yielding 100° stroke amplitude and symmetrical wing rotation at dorsal and ventral stroke reversal. Kinematic phase shift is the temporal offset between fore- and hindwing motion. (C) The shape of the robotic forewing and hindwing used. The wings are driven by servo motors mounted in a gear box that controls back/forth, up/down and rotational wing motion. Forces and moments acting on the wing during motion are measured on the surface mid point of the force sensor (blue circle). The center of gravity of the wing including the mass of the wing's holder is indicated by a red circle, respectively. l_x, length of the horizontal moment arm for the wing's center of gravitiy; l_y, length of the vertical moment arm between the wing's center of gravitiy and the wing's rotational axis. (D) Wing deflection due to bending moments under static load of the plexiglas model forewing (orange, red, black) and hindwing (cyan, green, blue). Deflection during load was measured at two distinct positions on the wing at two-third wing length (orange, cyan) and the wing tip (red, black, green, blue). To load the wing, small metal weights were placed on the upper wing surface either at two-third distance from the wing base (**, red, green, cyan, orange) or on the wing tip (*, black, blue). The vertical gray line indicates approximately mean force (0.3 N) measured throughout one complete stroke cycle on the wings during flapping motion. Horizontal gray area shows the range of deflections for fore- and hindwing, assuming the wing is loaded with mean force. The pictogram illustrates the measurement procedure showing wing holder and the wing seen parallel to the wing's surface.

in angle of attack are pronounced, particularly at the stroke reversals when the wing accelerates and decelerates during translational motion. Combining Equation 3 and the inertial forces produced during wing rotation thus yields for wing inertia in the horizontal (drag) stroke plane:

$$F_h(t) = F_h^*(t) + m_w l_y \ddot{\alpha} \sin\alpha . \qquad (5)$$

We calculated the contribution of wing inertia to total lift and drag forces separately (Fig. 2A). The data indicate that wing inertia appears to be small and may account solely for a small

fraction of the measured force at the beginning of the stroke cycle.

When a wing accelerates within the fluid it sets the surrounding air in motion, resulting in inertial forces by the fluid (added mass effect). Although added mass effects appear to be small during wing motion of a slightly larger *Drosophila* model wing that moves at similar speed and Reynolds number (Sane and Dickinson, 2001a), we calculated the potential contribution of added mass inertia using an analytical model for an infinitesimally thin 2D plate moving in an inviscid fluid
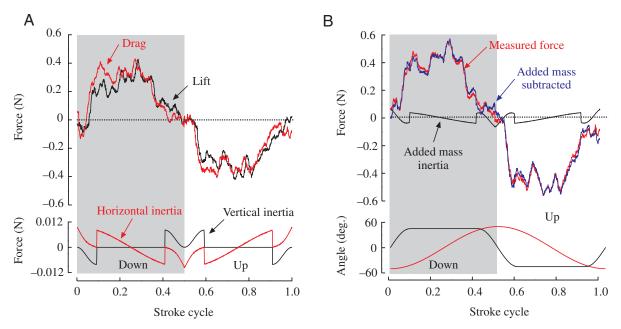
Fig. 2. Inertial forces during wing flapping due to wing mass (A) and added mass (virtual mass) of the wing (B). For kinematic details, see traces in B (bottom) and explanations given in the text. (A) Top: unfiltered raw force trace of lift (black) and drag (red) measured during a single stroke of the dragonfly model hindwing. Bottom: wing inertia in the horizontal (drag, red) and vertical (lift, black) calculated from the acceleration profile during translational and rotational wing motion of a complete stroke cycle. Total wing mass is equal to the mass of the wing and the holder attached to it. Note the different force scales. (B) Top: unfiltered total forces measured during wing motion of the model hindwing (red) within one flapping cycle with superimposed added mass inertia (black) calculated according to the equation given in the text. The blue trace shows the measured forces after subtracting added mass inertia. Bottom: kinematic pattern used for calculations of inertia. Traces show the angular position of the wing within the horizontal stroke plane (red) and the wing's angle of attack (black) throughout the entire stroke cycle.

modified towards 3D conditions using a blade-element approach (Sane and Dickinson, 2001a; Sedov, 1965). Similar to the wings of a fruit fly, the model wings used in this study rotate approximately at one quarter chord length from the leading edge. Total force normal to the wing surface due to the added mass acceleration of the fluid may be then expressed as (cf. erratum on equation 1 in Sane and Dickinson, 2001b, but additional corrections also apply; S. Sane, personal communication):

$$F_N(t) = \frac{1}{4}\left[\pi\rho R^2\bar{c}^2(\ddot{\phi}\sin\alpha+\dot{\phi}\dot{\alpha}\cos\alpha)\int_0^1 \hat{r}\hat{c}^2(\hat{r})\mathrm{d}\hat{r}\right]$$
$$+ \frac{1}{16}\left[\pi\rho R\bar{c}^3\ddot{\alpha}\int_0^1 \hat{c}^3(\hat{r})\mathrm{d}\hat{r}\right], \quad (6)$$

in which $\hat{c}(\hat{r})$ is the non-dimensional wing chord. The left integral we approximated to be 0.41 for the fore- and 0.45 for the hindwing, whereas the right integral is 1.29 and 1.13 for the two wings, respectively. We calculated added mass forces for each of the model wings using our generic kinematic pattern (Fig. 2B). Similar to wing inertia, added mass inertia seems to be relatively small and accounts for only small changes in the measured force trace. In our analysis on the significance of kinematic phase relationship we therefore made no attempt to correct the recorded data for inertial effects.

Reynolds number

In aerodynamics the fluid flow around a wing depends on *Re*, which is the ratio of inertial forces to viscous forces within the fluid. In flapping flight of insects this measure is conventionally defined by the product of mean wing chord and time-averaged wing tip velocity divided by the fluid's kinematic viscosity (Ellington, 1984c). Reynolds number for wing motion in our experiments was 105 for the forewing and 125 for the hindwing, which is thought to be at the lower end of *Re* observed for dragonflies (Rüppell, 1989). For example, the smallest dragonfly (*Nannophya pygmaea*), with a hindwing length of 10.5 mm, will fly at *Re*=250–500, assuming a stroke amplitude of 50–100° and a wingbeat frequency of 80 Hz. Reynolds number for wing motion of *Polycanthagyna melanictera* as shown in Fig. 1A is higher and amounts to approximately 2000 (Wakeling and Ellington, 1997). However, Kliss et al. (1989) modeled hovering dragonfly aerodynamic using a flat plate at *Re*=10–4300, as mentioned above. The difference in *Re* between our model wing of ~100 and an averaged sized dragonfly flying at *Re*>1000 appears to be important in this study and might be troublesome for interpreting the data. However, there are several reasons that the flow conditions at *Re*=100 are sufficiently similar to the flow conditions we expect at *Re*>1000. First, empirical data on static plates in uniform flow show that the force coefficients vary only little between *Re*=100 and 1000. Although this variation is slightly higher than the stable coefficients above

Re=1000, it is much less than between *Re*=10 and 100 (Hoerner, 1965). Most of the transition from attached flow conditions to flow separation at which flow is shed at reasonable intervals seems to happen within the range *Re*=10–100.

Second, the shedding frequency in static plates is a function of *Re* and changes in *Re* domain between 100 and 1000 that would be relevant for our experimental approach. The force coefficients of our model fore- and hindwing depend critically on the time of vortex shedding relative to the stroke reversals. However, the strong dependency of vortex shedding on *Re* is questionable in root-flapping wings at which the spanwise wing blade elements face different flow velocities and thus different *Re* during translatory motion. Previous studies using mechanical flappers have shown that root-flapping wings may stabilize a leading edge vortex (LEV), and vortex shedding at the stroke reversals at which the wing changes the sign of the angle of attack may occur before the vortex grows too large to be shed during wing translation (Birch and Dickinson, 2001). Moreover, a recent paper on LEV stability reported that even in a

continuous rotating propeller mimicking wing translation of the hawkmoth *Manduca sexta*, the LEV remains stable and no vortex shedding occurs, similar to those expected in a flat plate translating through the fluid at similar *Re* (Usherwood and Ellington, 2002a). Usherwood and Ellington (2002b) concluded that the shifts from early to steady flow conditions are relatively constant throughout a large range of *Re*. Thus it appears possible that the wings of a fruit fly *Drosophila* (*Re*=100–200) exhibit a similar force coefficient to the flapping wings of a quail (*Re*=26,000) because the high force coefficients in both animals are supposedly due to leading edge vorticity (Usherwood and Ellington, 2002b). This view is supported by an analytical model on flow separation (Miller and Peskin, 2004) suggesting that shedding behaviour in wings is only affected at *Re*<50, which is consistent with the experimental data on flat plate in uniform flow obtained by Hoerner (1965). In sum, all the above results suggest that investigating dragonfly wing–wake interaction at *Re*=100 seems to be less troublesome than would be expected from flat plate data. Moreover, the low *Re* used in this study was helpful for conducting DPIV because the high viscosity of the
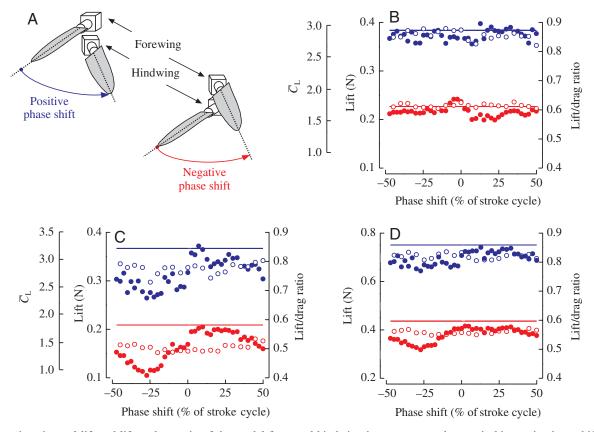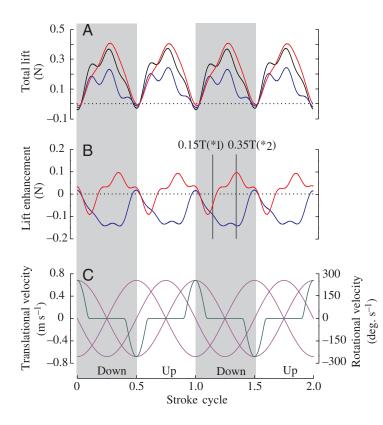

Fig. 3. Alterations in total lift and lift-to-drag ratio of the model fore- and hindwing in response to changes in kinematic phase shift between both wings. (A) Negative phase-shift values indicate that the forewing leads wing motion (red) throughout the entire stroke cycle whereas positive phase-shift values indicate that the hindwing leads wing motion (blue). Kinematic pattern of both wings is the same (cf. Fig. 4C). (B-D) Lift averaged over an entire stroke cycle (closed red circles) and lift-to-drag ratio (closed blue circles) are shown for the forewing flapping on top of the hindwing (B), the hindwing (C) and the combined performance of both fore- and hindwing (D) during various kinematic phase relationships. Performances of single wings flapping without wake–wing interaction are shown as solid lines in the respective color. Data are presented for the robotic wings vertically separated by 1.3 (closed circles) and 5.0 (open circles) mean forewing chord lengths, measured as the distance between the rotational axis of the two wings (cf. Fig. 1C). For an explanation of $\overline{C}_\mathrm{L}$, see text.

fluid (mineral oil, see below) minimized the buoyancy of the seeding particles (air bubbles) that we tested experimentally using different mineral oils. Thus, the *Re* selected in this experiment was the best compromise between matching the flow conditions to dragonfly hover flight between 1000 and 2000 and the experimental constraints on visualizing reliably the flow around the wings using DPIV.

Particle image velocimetry

To visualize wake structure, the oil was seeded with bubbles by pumping air through a ceramic water-purifier filter. The seeding consisted of evenly sized small bubbles with low upward velocity (<0.5 mm s⁻¹) and high concentration. We used a 50 mJ per pulse dual mini-Nd:YAG laser (Insight v. 5.1, TSI, Shoreview, MN, USA) to create two identical positioned light sheets approximately 5 mm thick separated in time by 2500 µs. Paired images of a 250 mm² flow field were captured using a PowerView 2M (TSI) camera. A two-frame cross-correlation of pixel intensity using the Hart Correlator engine (TSI) for a final interrogation area of 32×32 pixels, resulted in more than 10 000 vectors. Each DPIV experiment consisted of a seven-stroke wingbeat cycle, and the flow fields from the last five strokes were recorded, averaged and analyzed. No further smoothing was applied to the flow field vectors. The light sheet intersected the hindwing at 50% wing length, perpendicular to the long axis of the wing. DPIV analysis, including calculation of vorticity, was done using Insight v 5.1 and TSI macros in Tecplot v 9.0.

Results

Kinematic phase modulation

The combined lift forces on the fore- and hindwing show a strong sinusoidal relationship, with modulation of kinematic phase shift between both flapping wings (Fig. 3). Higher lift forces are produced when the hindwing leads and lower lift forces are produced when the forewing leads the stroke cycle. The 24% peak-to-peak modulation in total lift production {sine fit, $y=0.38+0.04\sin[\pi(x+6.2)/50]$, $\chi^2=0.17\times10^{-3}$; Fig. 3D, closed red circles} was accompanied by a modulation in lift-to-drag ratio of less than 10% {sine fit, $y=0.81+0.03\sin[\pi(x+1.2)/50]$, $\chi^2=0.17\times10^{-3}$; Fig. 3D, closed blue circles}. Unexpectedly, the combined fore- and hindwing peak lift is similar (within 4.6% accuracy) to the combined fore- and hindwing lift of the wings flapping separately (0.44 N; Fig. 3D, red line). Lift and drag modulation in fore- and hindwing vanished completely when the wings were separated vertically by more than 5 forewing chord widths (Figs 1C, 3B–D, open circles). At 5-chord-width distance to the forewing stroke plane, the temporal fluctuations in the fluid due to vortex shedding had ceased superficially and the downwash exhibited a temporal constant and homogenous velocity characteristics. Compared to a single wing, the vertical flow component at 5-chord distance reduced both the lift coefficient of the hindwing on average by 22% ($\overline{C}_L=1.43\pm0.007$, mean ± s.d., $N=20$ *vs* single wing $\overline{C}_L=1.84$; Fig. 3C) and the lift to drag ratio (L/D) of the hindwing by 8.3% (L/D=0.78±0.02, mean ± s.d., $N=20$ *vs* single wing L/D=0.84; Fig. 3C). In contrast, the forewing performance at 5-chord wing separation ($\overline{C}_L=1.76\pm0.03$, mean ± s.d., $N=20$, L/D=0.87; Fig. 3B) was approximately similar to the performance of a single flapping forewing ($\overline{C}_L=1.75$, L/D=0.86; Fig. 3B). All measured lift coefficients are well above the maximum 2D steady-state coefficients of artifical and real dragonfly wings (typically $\overline{C}_L=0.9–1.1$) measured under various conditions, indicating that a LEV has

Fig. 4. Maximum modulation in lift performance throughout a stroke cycle occurs during the second quarter of each half stroke. (A) Time history of lift forces in the robotic dragonfly hindwing during the stroke cycle are shown for stroke conditions in which the hindwing (red) or the forewing (blue) leads by a quarter stroke cycle. Lift of the hindwing free from forewing wake interference is plotted in black. (B) Lift enhancement on the hindwing calculated from the difference in performance between the hindwing with and without forewing wake interference (difference between colored and black line shown in A). Red (blue) line indicates lift enhancement when the hindwing (forewing) leads by a quarter stroke cycle. Asterisks *1 (15% stroke cycle) and *2 (35% stroke cycle) indicate the position in the stroke cycle when DPIV analysis was performed in Figs 7 and 8. (C) Translational (purple) and rotational (green) velocities of the wing (measured at the wing's second moment of area). The three translational plots represent the velocity profiles for the best (hindwing leads by 25% stroke cycle), zero (both wings move in-phase) and worst (forewing leads by 25% stroke cycle) kinematic patterns. T, stroke cycle.
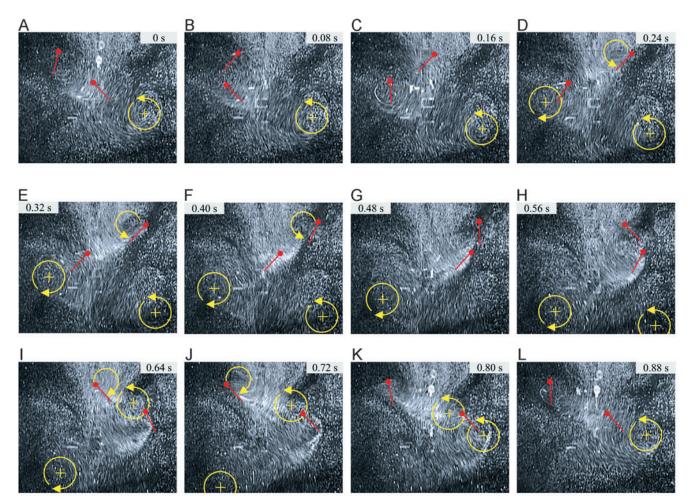
Fig. 5. (A–L) Time sequence of the wake produced by a tandem dragonfly model wing moving in a horizontal plane and highlighted by air bubbles in the mineral oil. The bubbles are illuminated by conventional fiber optics that intersect the wake at approximately 50% distance from the wing base and normal to the wing surface at mid half stroke. The red lines in each graph indicate inclination of the visible chordwise wing element as it appears on the video images; the upper and lower lines show wing motion of the forewing and hindwing, respectively. Leading wing edge is indicated by a red dot. (A–F) Complete half stroke (upstroke) of the forewing moving from left to right. (G–L) Complete half stroke (downstroke) of the forewing moving from right to left. The time sequence shows the wake while the forewing leads hindwing motion by a quarter stroke cycle. In all images yellow pictograms indicate the location and spin of vortices either shed in the wake (vortex core is marked by a cross) or attached to the wing (leading edge vortex). Only when clearly visible in the fluid, the vortices' spin and location were reconstructed from the video by eye and within the illuminated plane of the wake. Note: vortices that were masked by other flow structures or moving outside the imaging plane are not shown in this reconstruction. The stroke period for flapping motion is 0.96 s and stroke amplitude is 100°. See text for more details on stroke kinematics. Images were taken using a conventional 50 Hz video camera (Sony, TRV120E, Cologne, Germany).

enhanced aerodynamic force production (Okamoto et al., 1996). Although stroke kinematics was similar in the fore- and hindwing, we did not calculate an averaged lift coefficient for the combined wing performance because both wings have different shape and size.

Most of the modulation in the combined performance is due the modulation in hindwing lift, with only small changes in lift production of the forewing. Forewing lift ranges from approximately 0.20 N when the hindwing leads by 7–22% stroke cycle to 0.24 N when the forewing leads by 3.6% stroke cycle (Fig. 3B). The maximum mean lift coefficient of approximately 1.84 for the forewing is thus slightly higher and minimum mean lift coefficient of approximately 1.50 is slightly lower than the performance of a single wing (Fig. 3B).

Hindwing lift is modulated by approximately a factor of two {sine fit, $y=0.16+0.04\sin[\pi(x+4.2)/50]$, $\chi^2=0.08\times10^{-3}$; Fig. 3C, closed red circles} and produces maximum lift force (0.20 N) when the hindwing leads by around a quarter stroke cycle. In contrast to the forewing, we measured minimum hindwing lift (0.11 N) when the forewing leads by approximately a quarter stroke cycle (Fig. 3C). Maximum mean lift coefficient for the hindwing we determined to be approximately 1.77, whereas minimum lift coefficient was approximately 0.89. Hind wing lift-to-drag ratio is modulated between approximately 0.68 and 0.85 {sine fit, $y=0.76+0.06\sin[\pi(x+2.4)/50]$, $\chi^2=0.69\times10^{-3}$} when changing the kinematic phase relationships between both beating wings (Fig. 3C, closed blue circles).
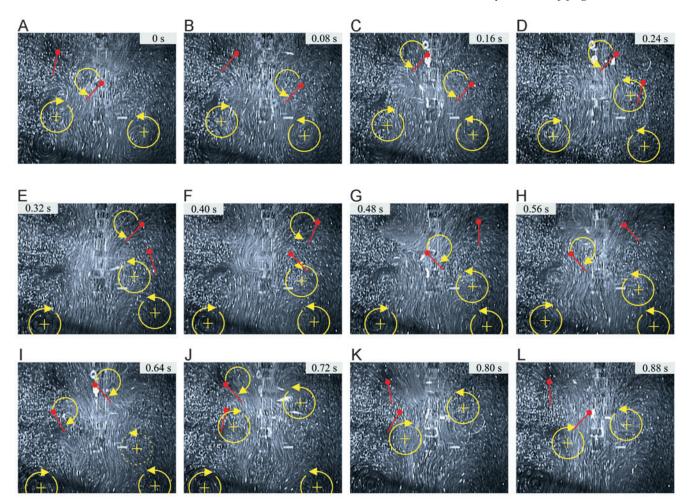
Fig. 6 (A–L) Time sequence of the wake produced by a tandem dragonfly wing moving in a horizontal plane. In contrast to Fig. 5, the time sequence shows the wake while the hindwing leads wing motion by a quarter stroke cycle. Wing kinematics and experimental techniques are similar to those mentioned in the legend for Fig. 5. The vortex that is indicated by the broken yellow line in I appeared to break down in the video image or moved outside the image plane.

Time traces of lift production

To uncover the aerodynamic mechanisms behind the phase modulation effects, we mapped the wing lift forces throughout a stroke cycle and identified positions where the interaction between the hindwing and the forewing wake has the largest effect on hindwing lift (Fig. 4). Due to stroke symmetry in both halfstrokes, the time course of force production is similar during the up- and downstroke and thus differs from the aerodynamic forces produced by a tethered dragonfly, flying with a steeply inclined stroke plane (Reavis and Luttges, 1988). Fig. 4A shows time traces of lift production for three different flapping conditions of the hindwing: hindwing lift free from forewing wake interference (black line), hindwing lift when the forewing leads by 25% stroke cycle (blue line) and hindwing lift when the hindwing leads by 25% stroke cycle (red line). The data show that positive lift is produced throughout the stroke with a small negative lift peak (lift force for all three cases = –0.013±0.003 N, mean ± S.D.) during wing rotation. Maximum lift forces of 0.37, 0.41 and 0.23 N were obtained just after the mid halfstroke (28% stroke cycle) for the three conditions: (i) single wing flapping,

(ii) hindwing leads and (iii) forewing leads wing motion by 25% stroke cycle, respectively. The difference between hindwing lift produced during the two different phase-shift relationships and the single wing performance is shown in Fig. 4B. In the best phase, when the hindwing leads by a quarter stroke, hindwing lift force is attenuated at the start of the stroke by approximately 0.10 N, but then develops a larger peak force (0.10 N) at a later position in the stroke cycle than a single hindwing free from forewing downwash (Fig. 4B, red trace). For the worst phase, when the forewing leads by a quarter stroke, lift throughout the stroke is considerably reduced, producing 0.14 N less lift at peak attenuation (Fig. 4B, blue trace). The worst phase peak attenuation, and the best phase peak enhancement both occur at approximately 35% and 85% of stroke cycle. The high magnitude of lift alteration and its dynamic change within the stroke cycle is thought to reflect major changes in the complex wake structure formed by the flapping wings.

Qualitative description of flow patterns

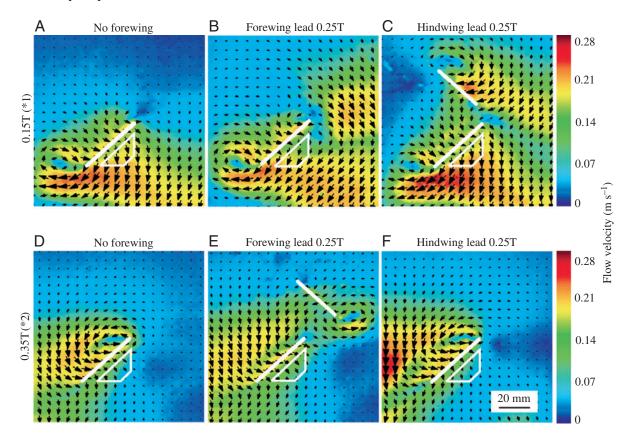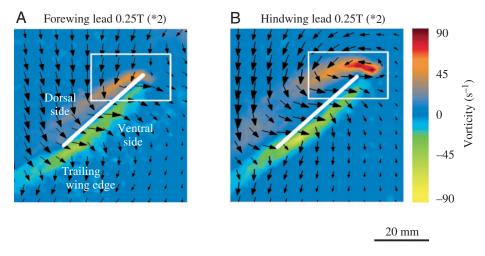To derive a course description of the flow structures that are

Fig. 7. Analysis of flow field velocities around the hindwing using DPIV techniques reveals the elaborate flow structures. The wing sections (white lines) are viewed at 50% distance between the wing base and tip, and have a geometric angle of attack of 45°. The direction of wing translation is from left to right in the hindwing (lower wing in panels) and, where present in the images, from right to left for the forewing (upper wing). The rotational axis for the fore- and hindwing is 0.33 and 0.22 chord widths, respectively. The DPIV images show wake velocity fields at two different times within the stroke cycle (A–C, 15% of stroke cycle; D–F, 35% of stroke cycle) when the hindwing flaps free from forewing downwash (A,D), when both wings flap but the forewing (B,E) or the hindwing (C,F) leads wing motion by a quarter stroke cycle. White open boxes in A–F indicate the region, located between the lower surface of the wing and the free stream, from which downwash flow velocities and angles were measured (see text for details). T, stroke cycle.

produced during wing–wake interference of the two ipsilateral wings, we visualized the moving air bubbles in the mineral oil using a conventional light source and fiber optics. The fiber optics were equipped with focusing lenses that allowed the illumination of an approximately 10 mm thick slice of the wake. The light sheet was oriented perpendicular to the moving wings at their midstroke position in each halfstroke, slicing the wings at approximately 50% wing length at this time. The time series, recorded by a conventional video camera, shows the wake: (i) when the forewing leads wing motion by a quarter-stroke cycle (Fig. 5) and (ii) when the hindwing leads by a quarter stroke cycle (Fig. 6). Within the illuminated plane we marked the spin and location of vortices only when they were clearly visible in the fluid. In some images, flow structures such as strong downwash or local density changes of the air bubbles masked the vortices, and we thus made no attempt to overlay the estimated position of the vortex in subsequent graphs. For example, in Fig. 5C we assume that the forewing has generated a leading edge vortex (LEV) at mid halfstroke, similar to the image 80 ms later (Fig. 5D); however, the strong downwash covered the view on

the forewing's LEV. At both kinematic conditions (forewing and hindwing lead by 25% of stroke cycle, respectively) we marked two different types of vortex structures in the wake: trailing edge vortices (starting vortex) shed at the beginning of wing acceleration after the wing has finished its rotation, and LEVs that develop on the upper wing surface during wing translation. The cores of the trailing edge vortices are marked by crosses in Figs 5 and 6. The wake when the forewing leads wing motion appears to be broader than the wake produced when the hindwing leads, indicating that in the first case the fluid is accelerated more strongly in a horizontal direction in each half stroke. This was quantified by the relative horizontal distance between the two prominent vortices that are visible downstream in the wake (Figs 5D–H, 6A–J). From Figs 5 and 6 we estimated that the wake close to the stroke plane is approximately 18% narrower when the hindwing leads compared to the wake produced when the forewing leads, a pattern that could explain the higher lift-to-drag ratio of hindwing lift when the hindwing leads by 25% of the stroke cycle (Fig. 3C). The vortex reconstruction of the wake highlights two interesting phases in which vortices are thought

Fig. 8. Vorticity contours near the hindwing with superimposed velocity vectors at 35% of stroke cycle when hindwing lift is enhanced or attenuated maximally (*2 in Fig. 4). Vorticity and velocity vectors for the kinematic condition in which (A) hindwing lift is attenuated maximally (worst condition; forewing leads by a quarter stroke cycle), and (B) hindwing lift exceeds lift production of a single hindwing flapping free of forewing downwash interference (best kinematic pattern; hindwing leads by a quarter stroke cycle). Square white boxes indicate the regions from which circulation of the leading edge vortex was measured. The wing sections (white lines) are viewed at 50% distance between the wing base and tip, and have a geometric angle of attack of 45°. The direction of wing translation is from left to right. T, stroke cycle.

to interact strongly. When the forewing leads, the trailing edge vortex is located near the leading wing edge of the hindwing (Fig. 5I–K). This might interfere potentially with LEV induction on the hindwing at the beginning of each halfstroke. In contrast, we did not observe such proximity between vortices yielding opposite spins when the hindwing leads wing motion by a quarter stroke cycle (Fig. 6). Due to the phase lead of the hindwing, the forwing's starting vortex seems to pass by near the left side (dorsal surface) of the hindwing at the end of the hindwing's translational phase (Fig. 6D). Interestingly, later in the stroke this vortex either breaks down in the downwash or moves outside the imaging plane (Fig. 6I, broken line of the vortex).
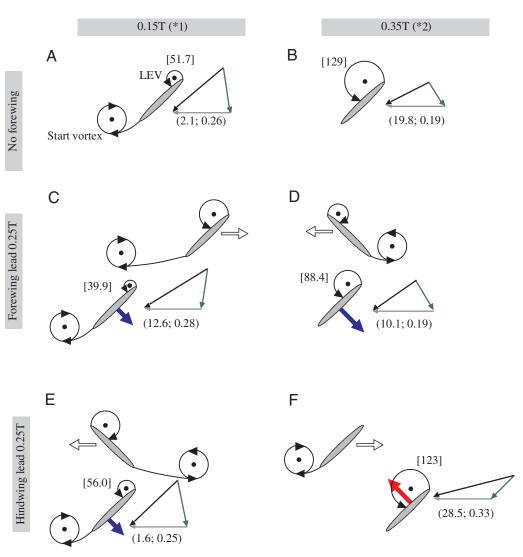
Particle image velocimetry

To gain more insights into the relationship between lift modulation and wake structure during wing–wake interaction, we characterized the flow conditions around the wings during both lift attenuation at the beginning of the stroke cycle (Figs 4B, 7, *1) and for the peak effects on lift later in the stroke (*2). As a first step, we mapped the potential alterations in the strength of the leading edge vortex on the hindwing in a defined region around the wing's leading edge using DPIV (Fig. 8, white box), because it has been shown previously that leading edge vorticity may contribute significantly to total lift production (Ellington et al., 1996; Polhamus, 1971; van den Berg and Ellington, 1997). As a second step, we derived the local flow conditions, including the effective angle of attack and the velocities of the wing relative to the surrounding oil, from DPIV analysis in a region between the free stream and the lower surface of the wing (Fig. 7, white box). The local flow conditions are of great importance since they determine the magnitude of lift production due to circulation bound to the wing during wing translation and circulation produced by the LEV, because total lift is proportional to the product of local flow velocity and circulation (Ellington, 1984b).

When the forewing leads by a quarter stroke cycle, the strength of the hindwing LEV is attenuated by 23% compared to a single wing flapping free of forewing wake interference, as measured at the beginning of the stroke cycle (Figs 4B, 7A,B, *1). The difference in vortex strength is even higher (31%) later in the stroke cycle (Figs 4B, 7D,E, 8, *2) after the wing segment has travelled approximately 1.2 chord widths after stroke reversal and the LEV has gained size. The smaller leading edge vorticity in the hindwing, when the forewing leads, coincides with the attenuation of lift in the stroke cycle, as shown in Fig. 4B. In contrast, the hindwing's LEV develops differently when the hindwing leads by a quarter stroke cycle. At both the early (15% of stroke cycle) and the late time (35% of stroke cycle) within each half stroke the hindwing's LEV achieves a strength similar to that of a flapping wing free of wake interference (Fig. 7A,C,D,F). This result suggests that, at least when the hindwing leads the stroke, the local flow conditions must have changed in order to explain both the lift attenuation at the beginning of the stroke (15% of stroke cycle) and the increases in instantaneous lift forces above the lift that can be achieved by single wing flapping at 35% of the stroke cycle (Fig. 4B).

To assess the effect of local flow conditions in order to explain the changes in lift production of the hindwing, we calculated the mean orientation of the flow towards the wing (effective angle of attack) and its mean velocities from the combined orientation and velocities of the downwash, and the motion and geometric angle of the wing, similar to a procedure suggested previously (Birch and Dickinson, 2001). At 15% of hindwing stroke cycle, the fluid vector reconstruction reveals that the effective angle of attack α_{eff} and flow velocities for the hindwing flapping in the forewing downwash, are favorable for the forewing leading phase (α_{eff}=12.6°; Fig. 9). In contrast, when the hindwing leads, the effective angle of attack decreases close to zero (α_{eff}=1.6°; Fig. 9). Local flow velocities remain approximately constant in all three cases (0.25–0.28 m s^{-1}; Fig. 9). Later in the hindwing stroke cycle (35% of stroke cycle) the local fluid vector is only favorable

Fig. 9. Schematic reconstruction of vortices and local flow conditions at two different kinematic phase relationships between fore- and hindwing and at two different times within the stroke cycle. Hindwing lift depends on LEV strength and the velocity and angle of the oncoming fluid (local flow). Local flow conditions (black vector) on the wing segment (grey oval) are calculated from the velocity and angle of the combined fore–hindwing downwash determined in a region below the wing's surface in a single PIV image plane (green vector, see white box in Fig. 7), and the translational velocity of the hindwing section (grey vector). Blue arrows, lift attenuation; red arrow (F), lift enhancement of the hindwing compared to a wing flapping free of forewing downwash. Vortical circulation ($cm^2 s^{-1}$) in the hindwing's leading edge vortex is shown in square brackets close to the LEV icon. The different strengths of starting and leading edge vorticies are indicated approximately by the size of the plotted 'vortex' icons. Effective angle of attack for the hindwing section (degrees, left value) and local flow velocity (m s^{-1}, right value) are shown respectively in parentheses under the vector diagram. (A–F) The flow characteristics for a flapping hindwing free from forewing downwash (single wing flapping) at (A) 15% and (B) 35% of stroke cycle; when the forewing (upper wing) leads wing motion by a quarter stroke cycle (C) at 15% and (D) 35% of stroke cycle; when the hindwing (lower wing) leads by a quarter stroke cycle (E) at 15% and (F) 35% of stroke cycle. A detailed description of vortex development and local flow is given in the text. In all diagrams, the motion of the hindwing (lower wing) is from left to right. White arrows indicate the direction of motion of the forewing. T, stroke cycle.

Discussion

The experiments using the physical model of a dragonfly have provided several new insights into how functionally four-winged insects might control lift production by varying the kinematic phase relationship between the fore and hindwing. Our results on a generic dragonfly stroke pattern show a marked modulation in hindwing lift and a small modulation in forewing lift on varying the phase-shift relationship between the fore- and hindwing stroke cycles (Fig. 3B–D). The maximum hindwing lift force is produced when the hindwing leads by around a quarter stroke cycle, corresponding to the phase-shift commonly used by locusts and dragonflies in climbing and forward flight (Alexander, 1984; Azuma and Watanabe, 1988; Baker and Cooter, 1979; Wakeling and Ellington, 1997; Wang et al., 2003; Weis-Fogh, 1956; Wortmann and Zarnack, 1993). Moreover, we have shown that the phase modulation effect on hindwing lift coincides with changes in the structure of the wake produced by the two beating wings. These changes cover alteration in leading edge vorticity (LEV destruction) on the hindwing and marked changes in the effective angle of attack and the magnitude of local flow velocities (Figs 7–9).

Wake structure in physical dragonfly models

The force measurements in our dragonfly model show that in a horizontal stroke, both half strokes contribute to aerodynamic lift production (Fig. 4). The major flow structures

for the hindwing leading case and not for the forewing leading phase, which matches the respective enhancement and attenuation of lift production in our direct force measurements.
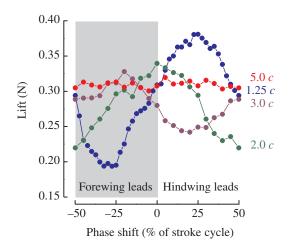
Fig. 10. Modulation of hindwing lift depends on the vertical distance between fore- and hindwing wing hinges. The traces show lift modulation similar to Fig. 3C for various distances between the wings measured in mean chord width *c*, while phase lag systematically varied between –50% (forewing leads by a half stroke cycle) and 50% (hindwing leads by a half stroke cycle). Aspect ratio of the two identical wings=2.7, stroke amplitude=120°, flapping frequency= 666 mHz, wing rotation symmetrical, *Re*=137.

we visualized in the wake are thus similar to the two major vortical structures found in other physical insect models, mimicking a 3D complete stroke cycle in the horizontal: a large starting vortex shed at the beginning of each half stroke and a leading edge vortex during wing translation (Figs 5 and 6; Birch and Dickinson, 2001; Dickinson et al., 1999; Ellington et al., 1996). Due to the complex flow pattern, we could not clearly identify stop vortices at the end of each half stroke. In contrast, Saharon and Luttges (1988) described eight vortices that are shed into the wake of flapping dragonfly model wings: four vortices by each wing throughout the stroke cycle. The authors found that each simple element of wing motion, such as the transition from pitching to plunging motion, initiated its own vortex structure. Similar patterns are described for vortex shedding patterns in a 2D model wing (Savage et al., 1979). Savage et al. found that a LEV (first vortex) is initiated during wing translation, which is common in most insect model wings moving at high angle of attack and similar to the present study (Birch and Dickinson, 2001; Ellington et al., 1996). During wing rotation (supination) for the subsequent half stroke, a second vortex is shed from the trailing wing edge in conjunction with trailing edge vorticity (third vortex) left in the wake in order to satisfy the Kutta condition when the wing starts to translate (Savage et al., 1979). In most cases, these vortex structures are displaced in the 3D model in the horizontal direction or move downstream when reduced frequency (based on wing beat/plunging cycle) is increasing from 0.18 to 5.0 (Saharon and Luttges, 1988). In many instances, however, the changes in vortex travel velocity were small, suggesting that there might be only minor alteration in overall wake pattern when the animal is changing forward speed (or reduced frequency; Saharon and Luttges, 1988).

Moreover, the smoke traces used to visualize the wake in the 3D dragonfly model suggested constructive vortex fusion that might amplify downwash patterns and enhance vortex persistence of the wings. In contrast, in the present robotic model we did not observe that vortices with the same spin fused in the wake, but found instead that hindwing LEV stability and persistence appears to be influenced by trailing edge vorticity shed from the forewing.

The robotic dragonfly model suggested by Saharon and Luttges (1988) differs from the present hovering model in several respects. First, Saharon's and Luttges' model was placed in a wind tunnel with a freestream velocity of 76 cm s^{-1}. From the data provided, we calculated a mean wing tip velocity of 540 cm s^{-1} that results in an advance ratio of approximately 0.14, whereas advance ratio in the present model is zero. Second, in addition to that, the robotic model of Saharon and Luttges mimicked the dragonfly kinematics during escape mode found by Norberg (1975), which is characterized by a highly inclined stroke plane while the dragonfly body is held horizontal. The tilted stroke plane, in turn, requires that a large proportion of total lift is produced during the downstroke at which the angle of attack of the hindwing is close to 90°, whereas during the upstroke the wing flapped at 0° angle of attack (fig. 3 in Reavis and Luttges, 1988). Third, the kinematic pattern shown by Saharon and Luttges suggests that the robotic model rotated its wings rapidly at the stroke reversals, when translational wing velocity was approaching zero. This kinematic pattern exhibited rather discrete translational and rotational phases, and this might be the reason why these authors found that each simple element of wing motion, such as the transition from pitching to plunging motion, initiated its own vortex structure. In contrast, the onset of wing rotation in our model wing began 10% of the stroke period prior a stroke reversal and ended 10% after the stroke reversal, which resulted apparently in a combined shedding of vortices produced during wing rotation and translation.

Changes in aerodynamic forces due to phase modulation

Phase modulation effects on the forewing were small and only occurred in phase-shift cases where the fore- and hindwing were moving close to each other throughout the stroke cycle (Fig. 3D). Thus it seems likely that some of the modulation of forewing lift is caused by wall effects due to physical distortion of forewing downwash by the hindwing (Dickinson et al., 1999; Rayner, 1991). We measured the maximum increase in forewing lift compared to the performance of a forewing flapping separately from the hindwing, when the forewing leads by 2.5–5% of stroke cycle. In this case the forewing downwash is directed completely onto the dorsal surface of the hindwing throughout the stroke cycle (Fig. 5). However, at most kinematic phase shifts we measured a small decrease in forewing lift, although hindwing downwash effects on forewing lift should be considerably less than forewing downwash effects on hindwing lift (Fig. 6). Two effects might be responsible for this difference. First, downwash flow velocities are thought to be considerably larger

below a wing than above it (Demoll, 1918; Hoff, 1919). Because the wing accelerates flow downwards, the resultant flow below the wing will have a smaller cross-sectional area than the flow above it, according to Venturi's principle, and consequently the flow velocities in the region below the wing will be higher than above. Thus, the high flow velocities in the forewing wing downwash potentially influence hindwing lift to a greater extent than the low flow velocities produced by the hindwing influence forewing lift. Second, the vortical structures in the wake travel in the direction of the fluid jet acceleration and thus it is likely that vortices shed by the hindwing have less interaction with the forewing than *vice versa*. Nevertheless, the small but significant modulation in forewing lift disappears when the two wing hinges are separated by more than 5 wing chords, supporting our hypothesis that forewing lift modulation might be due to wall effects caused by the hindwing (Fig. 3B, open red circles).

In contrast to the forewing, the stroke-phase relationship between both wings alters hindwing lift production by a factor of approximately 2 (Fig. 3C). Quite similar to the finding on forewing lift, the modulation ceases when we increase the distance in vertical separation between the two wing hinges, resulting in an approximately constant loss of hindwing lift production (Fig. 10). This result suggests that the phase modulation of hindwing lift production is likely to be due to transient forewing wake structures, because at 5-chord-width depth the forewing wake velocities are rather homogenized within the fluid. One potent transient vortex structure likely to influence hindwing lift is the forewing starting vortex that is left in wake while the traveling wing builds up aerodynamic circulation after starting from rest (Figs 5 and 6). Because of vortex interaction, we were not able to identify reliably the two vortices as single structures at all phases of the stroke cycle when flapping both wings; however, results obtained from so-called 'static' wing experiments might be able explain the relative decrease in leading edge vorticity of the hindwing, as shown in Fig. 8. We studied the potential threat of starting vortical structure on hindwing lift in DPIV experiments in which the hindwing remained static at its 15% of stroke cycle position throughout the forewing stroke (using identical fore- and hindwings, aspect ratio=3.6). These experimental conditions show that the position of the forewing's starting vortex is close to the hindwing's leading edge, next to the position of the developing LEV, potentially attenuating its development and thus decreasing hindwing lift.

The theoretical work by Lan (1979), who predicted that the optimum kinematics to maximize hindwing lift is a 25% phase shift, supports the finding in our physical dragonfly model but runs counter to lift measurements on a tethered flying dragonfly *Aeshna palmatta* (Reavis and Luttges, 1988). On the force balance, *Aeshna* (body weight 0.6 g) produces approximately 1.4 g lift when the 'beta angle' is ~87°. Reavis and Luttges (1988) defined the 'beta angle' as the angle between the freestream flow and the distance between the fore–aft wing tips. For this reason, the 'beta angle' is not identical with the phase-shift angle used in this study, although the 'beta angle'

appears to be a comparable measure for the kinematic phase difference between the two flapping wings. The force measured in the animal *increases* to approximately 3.7 g lift when the 'beta angle' *decreases* to a value of approximately 52°, which appears to be opposite to the finding in our dragonfly model. Nevertheless, the tethered flight data apparently indicate that a change in kinematic phase relationship between the fore- and hindwing may modulate total peak lift by a factor of 2.6. This value is approximately twice the modulation we found in the present study for the performance of the combined wings (Fig. 3D) and is close to the modulation we found for the hindwing (Fig. 3C). A possible explanation for the discrepancy in sign between the data derived from the dragonfly and the analytical/physical model is that while varying phase shift, the dragonfly modulates simultaneously other kinematic parameters such as stroke amplitude (varies in the hindwing between 60 and 75°), stroke frequency (varies between 34 and 37 Hz) and maximum angle of attack of both wings (forewing range is 65–90°, hindwing range is 35–55°; Reavis and Luttges, 1988). Since the force data derived from the tethered dragonfly imply that maximum lift increases linearly with an increase in all three kinematic parameters, a phase advance of the hindwing, in conjunction with a pronounced *decrease* in amplitude, frequency and/or angle of attack, would explain the decrease in lift measured in the tethered flying animal.

Regain of hindwing lift

Despite vortex interaction in the wake produced by the combined fore- and hindwing downwash it is remarkable that the hindwing, whilst flapping in the wake of the forewing, is able to restore lift to a level close (within 2.5%) to that of the hindwing flapping free from forewing downwash. Although this can only be achieved at a flapping condition where the hindwing motion leads by a quarter stroke cycle, it is quite unexpected because recent studies have shown that for two-winged hovering insects the first wingbeat produces more lift than subsequent wingbeats (Birch and Dickinson, 2001). A likely explanation of this finding is that the first stroke moves through undisturbed air and all subsequent strokes move through the downwash of the previous stroke, which may reduce lift by more than 10% (Birch and Dickinson, 2001). The same phenomenon is found in helicopter aerodynamics, where each rotor blade passes through the downwash generated by the preceding blade (Stepniewski and Keys, 1984). Closely related to helicopter technology (single and coaxial rotor blades) is the counter-rotating propeller technology (tandem propeller) in some long-range reconnaissance aircrafts such as the Shackleton. At small forward speeds, a single propeller imparts a significant amount of rotational flow to the air passing through the propeller disk. This rotational flow does not contribute to thrust, and lowers the lift-to-drag ratio and thus the efficiency of the aircraft. A second propeller close to the first propeller and turning in the opposite direction, however, may turn the rotational motion of the fluid into useful thrust, which appears to be widely related to the fluid dynamic

phenomena found in our root flapping dragonfly wings. Our direct force measurements show that the regain in hindwing lift in the dragonfly model results from a complex temporal pattern in which hindwing lift is attenuated at the early stroke phase (15% of stroke cycle) but then produces lift in excess of that produced by a wing flapping separately later in the half stroke cycle (35% of stroke cycle).

The estimates of wing inertia and added mass inertia as shown in Fig. 2 suggest that the alterations in hindwing lift are not easily attributable to inertial components because those components are typically less than 5% of the measured force. For this reason, it appears more likely that the changes in hindwing lift result from aerodynamic phenomena rather than from pronounced inertial effects. Thus to understand the nature of hindwing lift attenuation and enhancement for the best phase case in more detail, we estimated both leading edge vorticity and the local flow conditions, because lift depends on fluid velocity and circulation (Ellington, 1984b). At the early stage in the half stroke (at 15% of hindwing stroke cycle), the small change in effective angle of attack from 2.1° to 1.6° might explain why hindwing lift (Fig. 4B, blue trace, *1) slightly decreases compared to a single hindwing, because LEV circulation would be similar (Fig. 9A,E, 51.7 *vs* 56.0 cm^2 s^{-1}). Despite the reasonable development of LEVs, the small effective angles of attack raise the question of why the model hindwing produces such large lift during wing translation. One possible explanation is that we underestimated the effective angle of attack because of leading edge vorticity. A translating wing that produces leading edge vorticity, causes the oncoming flow to behave as it does around a cambered wing. A cambered wing, however, is able to generate large lift even at low geometrical angle of attack close to zero. Although this view might explain the elevated flight forces early in the stroke cycle (Fig. 4A, *1), it cannot easily explain the *difference* in hindwing lift production during one- and two-wing flapping conditions because leading edge vorticity is similar in both cases, as mentioned above (Fig. 9A,E). Instead, it appears likely that in the flapping tandem wings, subtle static pressure distributions (especially the expected over pressure on the lower forewing surface) might attenuate hindwing lift, which was not estimated in the present study.

A similar aerodynamic mechanism to that described above (change in effective angle of attack) appears to apply later in the stroke (at 35% hindwing stroke cycle), at which lift increases above single wing performance due to an increase in angle and magnitude of the local flow of approximately 70% and 58%, respectively, compared to the single wing, while leading edge vorticity is approximately equal in both flapping conditions (123 *vs* 129 cm^2 s^{-1}; Fig. 9B,F). To explain the favorable gain in local flow conditions for the hindwing, we suggest the following hypothesis. Fig. 5 shows that the downwash produced by the wings is not directed exactly vertically downward because the inclined wings pull the fluid into the direction of wing motion (*re-actio* component of drag). As a consequence, at stroke conditions in which the hindwing faces the forewing downwash produced in a preceding or subsequent halfstroke, the vector angle of the forewing downwash is less corruptive than the angle of the oncoming fluid when both wings translate in the same direction (Fig. 9C). The hindwing in Fig. 9F thus yields a high angle of incidence towards the oncoming flow (28.5°) because the local downwash is determined partly by the forewing downwash produced in the previous forewing halfstroke (cf. inclination of green arrows in Fig. 9). In addition to that, the velocity of the forewing downwash contributes to the flow velocity that the hindwing experiences while moving through the fluid, which in turn amplifies aerodynamic force production at this moment of the stroke cycle (Fig. 4B). Assuming that this explanation is valid, then we would also expect a favorable downwash at 35% downstroke cycle when the forewing leads wing motion, because at this moment the forewing downwash is thought to be directed similarly towards the hindwing (Fig. 9D). The reconstruction of local flow conditions, however, has shown that under these flow conditions the local flow vector points into the direction of the hindwing downwash (green arrow points in the direction of hindwing motion) and thus lowers the hindwing's effective angle of attack (Fig. 9D). A possible reason for this phenomenon is that the LEV on the forewing is not fully developed at this moment of the stroke, indicated by the small decrease in total lift at 25% kinematic phase lag (Fig. 3B). Therefore, we suggest that the decrease in aerodynamic performance of the forewing at 35% stroke cycle, due to a possible reduction in leading edge vorticity, might lower the hindwing's capability to produce lift because of unfavorable local flow conditions. We further assume that this hindwing–wake interaction might be highly sensitive to subtle changes in stroke kinematics that alter leading edge vorticity at the beginning of the stroke cycle, such as timing and speed of wing rotation during the ventral and dorsal stroke reversals. The dependency of hindwing lift modulation on stroke cycle timing, as shown by our generic kinematic model, might even indicate that by adjusting more kinematic parameters in the stroke cycle, a higher gain in lift performance might be achieved than the one shown here.

Wing–wake interaction between contralateral wings

The small stroke amplitude of typically 50–100° found in flying dragonflies limits the interaction of flow structures produced by the ipsilateral and contralateral wings because the biofoils are well separated during ventral and dorsal stroke reversal (Alexander, 1982, 1984, 1986; Azuma and Watanabe, 1988; Chadwick, 1940; Norberg, 1975; Reavis and Luttges, 1988; Rudolph, 1976a,b; Rüppell, 1985, 1989; Wakeling and Ellington, 1997; Weis-Fogh, 1967). High-speed film sequences of tethered flight kinematics in dragonflies show only one example in which the dragonflies *Libellula luctosa* and *Celithemis elisa* performed a physical interaction between the wings during the dorsal stroke reversal (Alexander, 1984). However, unlike dragonflies, damselflies typically show dorsal wing interaction and may use an unsteady lift enhancing mechanism termed the clap-and-fling or partial fling (Rudolph, 1976a,b; Wakeling and Ellington, 1997). For example, the

damselfly *Calopteryx splendens* performs the clap-and-fling similar to the motion of the wings described by Weis-Fogh (1973) for the small wasp *Encarsia formosa*. As the wing reaches the top of the upstroke, the upper wing surfaces meet and then, as the wings rotate and separate, air is drawn into the opening gap, enhancing wing circulation and thus wing lift (Bennett, 1977; Edwards and Cheng, 1982; Ellington, 1975; Lighthill, 1973; Maxworthy, 1979; Spedding and Maxworthy, 1986; Sunada et al., 1993; Weis-Fogh, 1973). In addition to damselflies, the clap-and-fling was found in various other insect species such as various Diptera (Ellington, 1984b; Ennos, 1989), lacewings (Antonova et al., 1981) and a whitefly (Wootton and Newman, 1979). It has been shown that insects performing clap-and-fling wing motion produce 25% more muscle mass-specific lift than insects flying with conventional wing beat (Marden, 1987). The clap-and-fling mechanism is not modelled by our generic kinematics for dragonfly because we employed solely two ipsilateral wings. Besides the clap-and-fling, a contralateral wing might also influence force production and thus phase-shift modulation of lift on an ipsilateral wing *via* the extension of LEV over the midline of the animal. This has been demonstrated in the red admiral butterfly *Vanessa atlanta*, flying freely in a wind tunnel with a free stream velocity at around 1–2 m s^{-1} (Srygley and Thomas, 2002). At the moment of take-off, the body angle of the animal with respect to the oncoming air and the wing's angle of attack approaches high values, supposedly inducing flow separation on the dorsal side of the body. As a consequence, the separation bubble on the dorsal body surface might facilitate the LEVs of both wings to expand over the body midline towards the contralateral wing. It remains open whether the qualitative description of flow pattern in the butterfly can be necessarily carried across to hovering flight in dragonflies at zero advance ratio, because under these conditions the wing root and the body of the animal only face the downwash that is orientated downwards and thus would be likely to initiate flow separation on the lower side of the animal's body. The high body angle and the relatively high flow velocity in the wind tunnel might, in case of the butterfly, provide an explanation for why the expansion of a LEV across the midline was not described in physical models that mimic hovering flight conditions in insects so far.

Concluding remarks

The present study on kinematic phase relationship in a hovering dragonfly model suggests that under certain kinematic conditions, lift production in tandem wings is maximized when the hindwing leads wing motion by approximately a quarter stroke cycle. It is possible that this result only holds for a limited range of wing kinematics and is limited to hovering flight conditions, although systematical variations in forward speed (reduced frequency) of the larger dragonfly model of Saharon and Luttges (1988) did not produce significant changes in flow structures. Additional flow components due to fast forward flight potentially influence local flow conditions, vortex initiation and vortex travel velocity in the wake produced by the wings (Wang, 2000a,b). To evaluate the robustness of our findings to changes in forward flight speed or reduced frequency, we simulated changes in vortex travel velocity by varying the vertical separation of the two wing hinges. The results in Fig. 10 show that the optimum phase relationship between two model wings (maximum hindwing lift) decreases with increasing distance between the two wings (peak force moves to the left). A possible explanation for this phenomenon is that the duration between the time at which the forewing sheds vortices and when those vortices interfere with the hindwing is increasing with increasing distance between the wings. This result implies that any change in stroke-phase relationship must be seen at least in conjunction with the magnitude of wing separation, because both kinematic parameters appear to determine the best phase for lift production in the tandem wing. The finding that the travel velocity of some vortices also depends on phase relationship (hindwing phase leads produces faster travel velocity due to an increase in downwash velocity) at constant wing separation might even complicate the aerodynamic consequences of the two kinematic parameters (Saharon and Luttges, 1989).

A similar picture might appear for aerodynamic effects due to more subtle changes in wing kinematics such as wing torsion, flexing, and changes in wing camber during flight (Song et al., 2001; Sunada et al., 1998), including effects due to corrugation of dragonfly wings (Kesel, 2000). Wing flexing, for example, has been discussed as a modification of the clap-and-fling termed the 'clap-and-peel', which might alter force production during the fling part of the wing motion (Ellington, 1984b). This modified clap-and-fling kinematics was found in fixed flying *Drosophila* (Götz, 1987) and larger insects such as butterflies (Brackenbury, 1991a; Brodsky, 1991), bush cricket, mantis (Brackenbury, 1990, 1991b), and locust (Cooter and Baker, 1977). In contrast, in our dragonfly model we used rigid flat plates that deformed only slightly during wing translation or wing rotation (Fig. 1D). Studies on the aerodynamic characteristics of dragonfly, for example, show that corrugated wings may have a slightly higher lift coefficient under 2D conditions than flat plates (Kesel, 2000; Okamoto et al., 1996).

In sum, we have shown that by using a generic stroke pattern derived from dragonfly kinematics, the phase relationship between a robotic fore- and hindwing may modulate hindwing lift force due to two separate, though not independent, effects. One seems to be the attenuation of hindwing leading edge vorticity (LEV destruction), and the second is the speed and angle of local flow conditions. The hindwing leading edge vorticity seems to be dependent upon hindwing proximity to the forewing starting vortex, the wing position within the stroke cycle and the local flow conditions. Timing between the fore- and hindwing can modulate the wake interference effects and can achieve instantaneous lift force greater than that achieved by a wing free from wake interference. The small decrease in lift-to-drag ratio does not necessarily imply that there is a small energetic cost associated with having two pairs of wings, because profile costs depend on the product between

wing velocity and drag (Fig. 3D). This issue of the fluid dynamics in four-winged insects we will address in a subsequent paper on the power requirements and aerodynamic efficiency of root-flapping tandem wings. The major benefit from the ability to modulate forces through fore- and hindwing phase relationships might be that it allows an insect to control lift production without further changes in stroke kinematics, thus offering an additional parameter for flight control. As suggested by several previous studies, right–left asymmetry in phase shift might allow functionally four-winged insects the ability to modulate forces asymmetrically, and this might explain why many dragonflies have been reported to vary phase shift during some turning maneuvers (Alexander, 1986; Norberg, 1975; Reavis and Luttges, 1988; Rüppell, 1989).

List of symbols

c	mean chord width
$\hat{c}(\hat{r})$	non-dimensional wing chord
$\overline{C}_L$	mean lift coefficient
DPIV	digital particle image velocimetry
F_h	horizontal inertial force due to wing translation and rotation
F_h^*	inertial force due to wing translation
F_v	vertical inertial force
$\overline{L}$	lift of a single wing averaged throughout the stroke cycle
LEV	leading edge vortex
L/D	lift to drag ratio
l_x	moment arm between the force sensor and the wing's center of mass
l_y	moment arm normal to the wing's rotational axis
m_w	wing mass
n	stroke frequency
r	radius
R	wing length
Re	Reynolds number
S	total wing area
T	stroke cycle
t	time
$\Delta\tau$	flip duration
Φ	stroke amplitude
α	angle of attack
ϕ	angular wing position during the stroke
ρ	density
τ_0	fraction of wing cycle time

References

Alexander, D. E. (1982). *Studies in Flight Control and Aerodynamics in Dragon Flies*. Durham: Duke University.

Alexander, D. E. (1984). Unusual phase relationships between the forwings and hindwings in flying dragonflies. *J. Exp. Biol.* **109**, 379-383.

Alexander, D. E. (1986). Wind tunnel studies of turns by flying dragonflies. *J. Exp. Biol.* **122**, 81-98.

Antonova, O. A., Brodsky, A. K. and Ivanov, V. D. (1981). Wing beat kinematics of five insect species. *Zool. Zh.* **60**, 506-518.

Azuma, A. and Watanabe, T. (1988). Flight performance of a dragonfly. *J. Exp. Biol.* **137**, 221-252.

Azuma, A., Azuma, S., Watanabe, I. and Furuta, T. (1985). Flight mechanics of a dragonfly. *J. Exp. Biol.* **116**, 79-107.

Baker, P. S. and Cooter, R. J. (1979). The natural flight of the migratory locust, *Locusta migratoria L.* – Wing movement. *J. Comp. Physiol.* **131**, 79-87.

Bennett, L. (1977). Clap-and-fling aerodynamics – an experimental evaluation. *J. Exp. Biol.* **69**, 261-272.

Bertin, J. L. and Smith, M. L. (1979). *Aerodynamics for Engineers.* Englewood Cliffs, NJ: Prentiss-Hall, Inc.

Birch, J. M. and Dickinson, M. H. (2001). Spanwise flow and the attachmant of the leading-edge vortex on insect wings. *Nature* **412**, 729-733.

Brackenbury, J. (1990). Wing movements in the bush cricket *Tettigonia viridissima* and the mantis *Ameles spallanziana* during natural leaping. *J. Zool. Lond.* **220**, 593-602.

Brackenbury, J. (1991a). Kinematics of take-off and climbing flight in butterflies. *J. Zool. Lond.* **224**, 251-270.

Brackenbury, J. (1991b). Wing kinematics during natural leaping in the mantids *Mantis religiosa* and *Iris oratoria. J. Zool. Lond.* **223**, 341-356.

Brodsky, A. K. (1991). Vortex formation in the tethered flight of the peacock butterfly *Inachis io* L. (Lepidoptera, Nymphalidae) and some aspects of insect flight evolution. *J. Exp. Biol.* **161**, 77-95.

Chadwick, L. E. (1940). The wing motion of the dragonfly. *Bull. Brooklyn Ent. Soc.* **35**, 109-112.

Chadwick, L. E. (1953). The motion of the wings. In *Insect Physiology* (ed. K. D. Roeder), pp. 577-614. New York: John Wiley and Sons.

Clark, H. W. (1940). The adult musculature of the anisopterous dragonfly thorax (Odonata, Anisoptera). *J. Morph.* **67**, 523-565.

Cooter, R. J. and Baker, P. S. (1977). Weis-Fogh clap-and-fling mechanism in *Locusta. Nature* **269**, 53-54.

Demoll, R. (1918). *Der Flug der Insekten und Vögel*. Jena: G. Fisher.

Dickinson, M. H., Lehmann, F.-O. and Götz, K. G. (1993). The active control of wing rotation by *Drosophila. J. Exp. Biol.* **182**, 173-189.

Dickinson, M. H., Lehmann, F.-O. and Sane, S. (1999). Wing rotation and the aerodynamic basis of insect flight. *Science* **284**, 1954-1960.

Edwards, R. H. and Cheng, H. K. (1982). The separation vortex in the Weis-Fogh circulation-generation mechanism. *J. Fluid Mech.* **120**, 463-473.

Ellington, C. P. (1975). Non-steady-state aerodynamics of the flight of *Encarsia formosa*. In *Symposium on Swimming and Flying in Nature. 2* (ed. T. Y. Wu), pp. 729-762. Passadena, California.

Ellington, C. P. (1984a). The aerodynamics of insect flight. II. Morphological parameters. *Phil. Trans. R. Soc. Lond. B* **305**, 17-40.

Ellington, C. P. (1984b). The aerodynamics of insect flight. IV. Aerodynamic mechanisms. *Phil. Trans. R. Soc. Lond. B* **305**, 79-113.

Ellington, C. P. (1984c). The aerodynamics of insect flight. VI. Lift and power requirements. *Phil. Trans. R. Soc. Lond. B* **305**, 145-181.

Ellington, C. P. (1984d). The arodynamics of hovering insect flight. I. The quasi-steady analysis. *Phil. Trans. R. Soc. Lond. B* **305**, 1-15.

Ellington, C. P., Berg, C. v. d., Willmott, A. P. and Thomas, A. L. R. (1996). Leading-edge vortices in insect flight. *Nature* **384**, 626-630.

Ennos, A. R. (1989). The kinematics and aerodynamics of the free flight of some Diptera. *J. Exp. Biol.* **142**, 49-85.

Gorb, S. (2001). *Attachment Devices of Insect Cuticle*, pp. 305: Kluwer Academic.

Götz, K. G. (1987). Course-control, metabolism and wing interference during ultralong tethered flight in *Drosophila melanogaster. J. Exp. Biol.* **128**, 35-46.

Grodnitsky, D. L. and Morozov, P. P. (1992). Flow visualization experiments on tethered flying green lacewings *Chrysopa Dasyptera. J. Exp. Biol.* **169**, 143-163.

Hoerner, S. F. (1965). *Fluid Dynamic Drag: Practical Information on Aerodynamic Drag and Hydrodynamic Resistance*. Brick Town, New Jersey: Hoerner Fluid Dynamics.

Hoff, W. (1919). Der Flug der Insekten und Vögel. *Die Naturwissenschaften* **10**, 159-162.

Kesel, A. B. (2000). Aerodynamic characteristics of dragonfly wing sections compared with technical airfoils. *J. Exp. Biol.* **203**, 3125-3135.

Kliss, M., Somps, C. and Luttges, M. W. (1989). Stable vortex structures: a flat plate model of dragonfly hovering. *J. Theor. Biol.* **136**, 209-228.

Lan, C. E. (1979). The unsteady quasi-vortex-lattice method with applications to animal propulsion. *J. Fluid Mech.* **93**, 747-765.

Lehmann, F.-O. and Dickinson, M. H. (1998). The control of wing kinematics and flight forces in fruit flies (*Drosophila* spp.). *J. Exp. Biol.* **201**, 385-401.

Lighthill, M. J. (1973). On the Weis-Fogh mechanism of lift generation. *J. Fluid Mech.* **60**, 1-17.

Marden, J. H. (1987). Maximum lift production during takeoff in flying animals. *J. Exp. Biol.* **130**, 235-258.

Maxworthy, T. (1979). Experiments on the Weis-Fogh mechanism of lift generation by insects in hovering flight Part 1. Dynamics of the 'fling'. *J. Fluid Mech.* **93**, 47-63.

May, M. L. (1995). Dependence of flight behavior and heat production on air temperature in the Green Darner dragonfly *Anax junius* (Odonata: Aeshnidae). *J. Exp. Biol.* **198**, 2385-2392.

Miller, L. A. and Peskin, C. S. (2004). When vortices stick: an aerodynamic transition in tiny insect flight. *J. Exp. Biol.* **207**, 3073-3088.

Milne-Thomson, L. M. (1966). *Theoretical Aerodynamics*, pp. 210-211. New York: Macmillan.

Mises, R. v. (1959). *Theory of Flight*. New York: Dover Publications, Inc.

Newman, B. G., Savage, S. B. and Scgouella, D. (1977). Model tests on a wing section of an *Aeschna* Dragonfly. In *Scale Effects in Animal Locomotion* (ed. T. J. Pedley) , pp. 445-477. London: Academic Press.

Norberg, R. A. (1975). Hovering flight of the dragonfly *Aeschna juncea* L. In *Kinematics and Aerodynamics*, vol. 2 (ed. T. Y.-T. Wu, C. J. Brokaw and C. Brennen), pp. 763-781. NY: Plenum Press.

Okamoto, M., Yasuda, K. and Azuma, A. (1996). Aerodynamic characteristics of the wings and body of a dragonfly. *J. Exp. Biol.* **199**, 281-294.

Polhamus, E. C. (1971). Predictions of vortex-lift characteristics by a leading-edge suction analogy. *J. Aircraft* **8**, 193-199.

Rayner, J. M. V. (1991). On the aerodynamics of animal flight in ground effect. *Phil. Trans. R. Soc. Lond. B* **334**, 119-128.

Reavis, M. A. and Luttges, M. W. (1988). Aerodynamic forces produced by a dragonfly. *AIAA J.* **88-0330**, 1-13.

Rudolph, R. (1976a). Die aerodynamische Eigenschaften von *Calopteryx splendens* (Harris) (Zygoptera: Calopterygidae). *Odonatologica* **5**, 383-386.

Rudolph, R. (1976b). Some aspects of wing kinematics in *Calopteryx splendens* (Harris) (Zygoptera: Calopterygidae). *Odonatologica* **5**, 119-127.

Rüppell, G. (1985). Kinematic and behavioral aspects of flight of the male Banded Agrion, *Calopterx (Agrion) splendens* L. In *Insect Locomotion* (ed. G. Wendler and M. Gewecke), pp. 195-204. Berlin: Paul Parey.

Rüppell, G. (1989). Kinematic analysis of symmetrical flight manoeuvres of Odonata. *J. Exp. Biol.* **144**, 13-42.

Rüppell, G. and Hilfert, D. (1993). The flight of the relict dragonfly *Epiophlebia superstes* (Selys) in comparison with that of modern Odonata (Anisozygoptera: Epiophlebiidae). *Odonatologica* **22**, 295-309.

Saharon, D. and Luttges, M. W. (1987). Three-dimensional flow produced by a pitching-plunging model dragonfly wing. *AIAA J.* **87-0121**, 1-17.

Saharon, D. and Luttges, M. W. (1988). Visulaziation of unsteady separated flow produces by mechanically driven dragonfly wing kinematics model. *AIAA J.* **88-0569**, 1-23.

Saharon, D. and Luttges, M. W. (1989). Dragonfly unsteady aerodynamics: The role of the wing phase relationship in controlling the produced flows. *AIAA J.* **89-0832**, 1-19.

Sane, S. and Dickinson, M. H. (2001a). The control of flight force by a flapping wing: lift and drag production. *J. Exp. Biol.* **204**, 2607-2626.

Sane, S. and Dickinson, M. H. (2001b). Erratum. *J. Exp. Biol.* **204**, 3401.

Sato, M. and Azuma, A. (1997). The flight performance of a damselfly *Ceriagrion melanurum* Selys. *J. Exp. Biol.* **200**, 1765-1779.

Savage, S. B., Newman, B. G. and Wong, D. T.-M. (1979). The role of vortices and unsteady effects during the hovering flight of dragonflies. *J. Exp. Biol.* **83**, 59-77.

Sedov, L. I. (1965). *Two-dimensional Problems in Hydrodynamics and Aerodynamics,* pp. 20-30. New York: Interscience Publishers.

Simmons, P. (1977a). The neuronal control of dragon flight. II. Physiology. *J. Exp. Biol.* **71**, 141-155.

Simmons, P. (1977b). The neuronal control of dragonfly flight. I. Anatomy. *J. Exp. Biol.* **71**, 123-140.

Somps, C. and Luttges, M. (1985). Dragonfly flight: novel uses of unsteady separated flows. *Science* **228**, 1326-1329.

Song, D., Wang, H., Zeng, L. and Yin, C. (2001). Measuring the camber deformation of a dragonfly wing using projected comb fringe. *Rev. Sci. Inst.* **72**, 2450-2454.

Spedding, G. R. and Maxworthy, T. (1986). The generation of circulation and lift in a rigid two-dimensional fling. *J. Fluid Mech.* **165**, 247-272.

Srygley, R. B. and Thomas, A. L. R. (2002). Unconventional lift-generating mechanisms in free-flying butterflies. *Nature* **420**, 660-664.

Stepniewski, W. Z. and Keys, C. N. (1984). *Rotary-Wing Aerodynamics,* vol. 1 + 2, pp. 236. New York: Dover Publications.

Sunada, S., Kawachi, K., Watanabe, I. and Azuma, A. (1993). Fundamental analysis of three-dimensional 'near fling'. *J. Exp. Biol.* **183**, 217-248.

Sunada, S., Zeng, L. and Kawachi, K. (1998). The relationship between dragonfly wing structure and torsional deformation. *J. Theor. Biol.* **193**, 39-45.

Usherwood, J. R. and Ellington, C. P. (2002a). The aerodynamic of revolving wings. I. Model hawkmoth wings. *J. Exp. Biol.* **205**, 1547-1564.

Usherwood, J. R. and Ellington, C. P. (2002b). The aerodynamics of revolving wings. II. Propeller force coefficients from mayfly to quail. *J. Exp. Biol.* **205**, 1565-1576.

van den Berg, C. and Ellington, C. P. (1997). The three-dimensional leading-edge vortex of 'hovering' model hawkmoth. *Phil. Trans. R. Soc. Lond. B* **352**, 329-340.

Wakeling, J. M. (1993). Dragonfly aerodynamics and unsteady mechanisms: a review. *Odonatologica* **22**, 319-334.

Wakeling, J. M. and Ellington, C. P. (1997). Dragonfly Flight. II. Velocities, accelerations, and kinematics of flapping flight. *J. Exp. Biol.* **200**, 557-582.

Wang, H., Zeng, L., Liu, H. and Chunyong, Y. (2003). Measuring wing kinematics, flight trajectory and body attitude during forward flight and turning maneuvers in dragonflies. *J. Exp. Biol.* **206**, 745-757.

Wang, Z. J. (2000a). Two dimensional mechanism for insect hovering. *Phys. Rev. Lett.* **85**, 2216-2219.

Wang, Z. J. (2000b). Vortex shedding and frequency selection in flapping flight. *J. Fluid Mech.* **410**, 323-341.

Weis-Fogh, T. (1956). Biology and physics of locust flight. II. Flight performance of the desert locust (*Schistocera gregaria*). *Phil. Trans. R. Soc. Lond. B* **239**, 459-510.

Weis-Fogh, T. (1967). Respiration and tracheal ventilation in locusts and other flying insects. *J. Exp. Biol.* **47**, 561-587.

Weis-Fogh, T. (1973). Quick estimates of flight fitness in hovering animals, including novel mechanisms for lift production. *J. Exp. Biol.* **59**, 169-230.

Wilson, D. M. (1968). The nervous control of insect flight and related behaviours. *Adv. Insect Physiol.* **5**, 289-338.

Wootton, R. J. and Newman, D. J. S. (1979). Whitefly have the highest contradiction frequencies yet recorded in non-fibrillar flight muscles. *Nature* **280**, 402-403.

Wortmann, M. and Zarnack, W. (1993). Wing movements and lift regulation in the flight of desert locusts. *J. Exp. Biol.* **182**, 57-69.